Vol. 15, No. 1 (2026): 419 - 430 http://dx.doi.org/10.23960/jtepl.v15i1.419-430

JURNAL TEKNIK PERTANIAN LAMPUNG

ISSN 2302-559X (print) / 2549-0818 (online)
Journal homepage : https://jurnal.fp.unila.ac.id/index.php/JTP

Simulation of Design Flood Discharge under Projected Land Cover Scenarios Using ANN–MOLUSCE and HEC-HMS in the Cijangkelok Watershed

Vika Febriyani[2,✉], Yadi Suryadi[1], Tri Wahyudin Ahmad[2], Arief Yudho Wicaksono[2], Yosephina Puspa Setyoasri[2]

[1] Water Resource Engineering Research Group, Faculty of Civil and Environmental Engineering, Institut Teknologi Bandung, INDONESIA

[2] Master Program of Water Resources Engineering, Faculty of Civil and Environmental Engineering, Institut Teknologi Bandung, INDONESIA.

Article History:

Received : 03 October 2025
Revised : 08 October 2025
Accepted : 03 November 2025

Keywords:

Cijangkelok River,
Flood discharge,
HEC-HMS,
Land cover,
MOLUSCE.

Corresponding Author:
✉ vikafebri@gmail.com
(Vika Febriyani)

ABSTRACT

River flooding during rainy season is partly resulted from land cover changes. This study analyzes the impact of land cover changes on flood hydrographs using Curve Number (CN), Impervious (I), and Initial Abstraction (Ia). Land cover data (2009 and 2022) were obtained from the Ministry of Environment and Forestry, while the 2035 scenario was modeled with QGIS MOLUSCE (ANN). CN and I values were then applied in HEC-HMS simulations with SCS and Snyder Unit Hydrograph methods. Results show major land conversion by 2035 is particularly from dryland to rice fields, built-up areas, and forest plantations. The 2035 land cover prediction had minimum overall error of 0.0332 and Kappa coefficient of 0.765, indicating good model reliability. Composite CN increased from 67.9 (2009) to 68.0 (2022) and 68.4 (2035); I values from 5.6 to 5.7 and 6.4; while Ia decreased from 24.0 to 23.9 and 23.5 (2035). Flood discharges with the SCS method rise from 617.2 m³/s (2009) to 623.8 m³/s (2022) and 641.3 m³/s (2035), while the Snyder method produced 621.3, 621.6, and 630.5 m³/s. Statistical comparison between simulated and frequency-based design flood discharge results in PBIAS values of 0.1–0.2 (very good) and NSE of 1.0 (very good). The discharge increases of 1.1–2.8% indicate that land cover changes contribute to higher flood potential, but still in moderate level as most conversion is to rice fields, which function as temporary water storage and delay direct runoff.

1. INTRODUCTION

Flooding is recognized as one of the most common and hazardous natural disasters worldwide. In Indonesia, it has been the most frequently occurring disaster since 2009 (Yoani *et al*., 2023). Flood in West Java can be attributed to long-term changes in climate and land cover, where land cover change has been the more influential factor (Rahayu *et al*., 2023). Land cover change affects infiltration, interception, evapotranspiration, groundwater recharge, and surface water storage in the terrestrial cycle, ultimately influencing runoff (He *et al*., 2021).

The Cijangkelok River, a tributary of the Cisanggarung River, frequently overflows during the rainy season, causing flooding in several villages along its course. According to data from the Flood and Drought Control Infrastructure Management Unit of BBWS Cimanuk Cisanggarung, the Cijangkelok River overflowed in 2017, 2018, 2020, 2021, and 2023, inundating nearby villages with water levels reaching up to approximately 1.5 meters.

The Cijangkelok River does not have sufficient capacity to handle hydrological discharge. Field surveys showed sediment build-up and siltation, uneven embankments, and land-cover changes in the surrounding area, all of which affect the river's condition and performance (Sjarief & Lasminto, 2020). Flooding is predominantly driven by natural

factors, especially prolonged high-intensity rainfall. However, human activities also contribute significantly, particularly through improper land cover practices (Anggista *et al*., 2025; Carsono, 2021).

This study aims to quantify the magnitude of flood discharge change under historical and projected land cover scenarios in the Cijangkelok River. The findings are expected to support flood mitigation planning in the Upper Cijangkelok River area and provide input for future land cover management strategies.

2. MATERIALS AND METHODS

The Cijangkelok Watershed has an area of 165.8 km² with a main river length of 36.6 km, discharging into the Cisanggarung River. In this study, the watershed outlet is limited to the Cibendung water gauge station (±11 km upstream from the confluence with the Cisanggarung), resulting in a study area of 147.1 km² with a river length of 25.6 km.

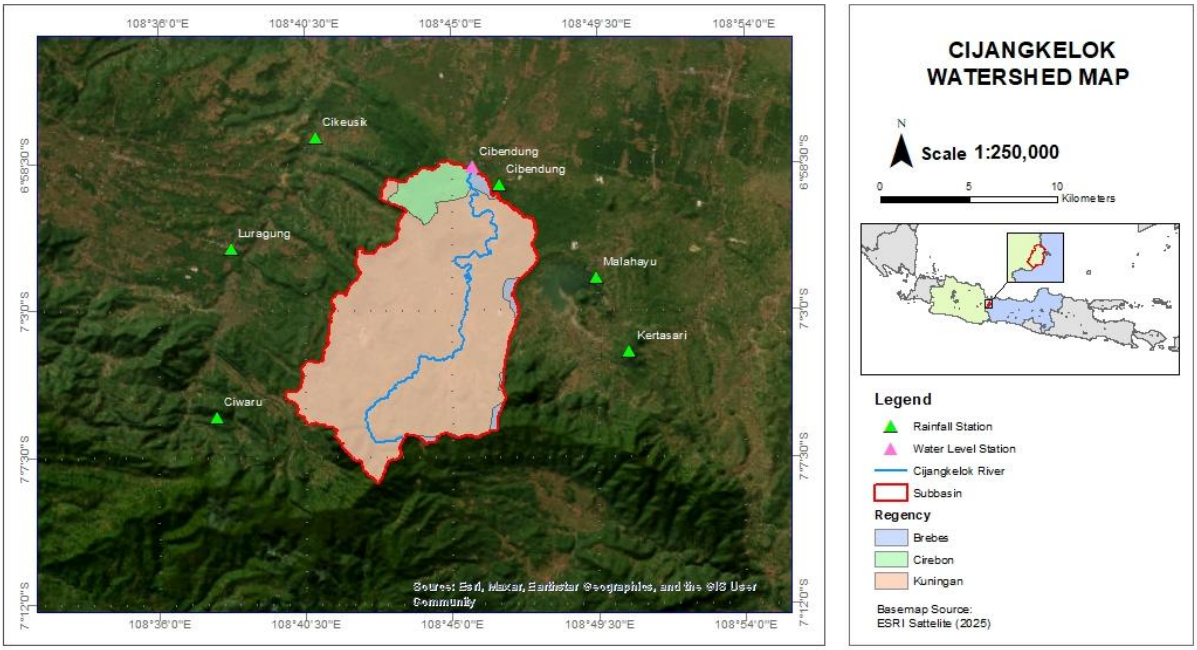

Figure 1. Cijangkelok Watershed

This watershed is located in Cirebon and Kuningan Regencies, West Java Province (97.3%) and Brebes Regency, Central Java Province (2.7%). The Cijangkelok River passes through 14 villages: Cimara, Cukarapih, Ciangir, Sumurwiru, Sukamaju, Sindangjawa, Cipondok, Sukaharja, Cibingbin, Cintenjo, Dukuhbadag, Bantarpanjang, Tonjong, and Cibendung.

2.1. Materials

The study on the impact of land cover change on flood hydrographs employs a descriptive-analytical approach. The data required to accomplish this research are as follows:

a. Rainfall data collected during 2005–2024 (20 years), collected from six rainfall stations distributed around the Cijangkelok watershed, namely Ciwaru, Luragung, Cikeusik, Cibendung, Malahayu, and Kertasari. The data were obtained from the Public Works and Spatial Planning Agency of Kuningan and Brebes Regencies, and BBWS Cimanuk Cisanggarung.
b. Observed discharge data collected during 201 1–2024 (14 years) from the Cibendung water level station, obtained from BBWS Cimanuk Cisanggarung.

c. Topographic data, obtained from the DEMNAS website (https://tanahair.indonesia.go.id/portal-web) and processed using ArcGIS software.
d. Land cover data for the years 2009 and 2022, obtained from the Ministry of Environment and Forestry.
e. Soil type map, obtained from the FAO Harmonized World Soil Database (HWSD) website available from https://gaez.fao.org/pages/hwsd.

2.2. Methods

To complete this study, several stages of analysis were conducted. The main methodological steps were outlined as follows:

2.2.1. Land Cover Prediction Analysis

Land cover prediction analysis was conducted using the Artificial Neural Network (ANN) method through the Modules for Land Use Change Evaluation (MOLUSCE) plugin in QGIS. This plugin is an open-source model available for QGIS version 2.0 and above, designed to analyze, model, and simulate land use/land cover changes using algorithmic modules, including artificial neural networks (ANN) (Muhammad *et al*., 2022). MOLUSCE trains an ANN-Multi Layer Perceptron model to learn transition patterns from the initial to the final condition in order to project future land cover (Kamaraj & Rangarajan, 2022). The driving variables used were the distance to roads, distance to rivers, and distance to built-up areas. The correlation among these variables was examined using Pearson's correlation method. Pearson's correlation coefficient (r) represents both the strength and direction of a linear association between two variables. It is calculated by dividing the covariance of the variables by the product of their standard deviations. The coefficient ranges from –1.0 to +1.0, where –1.0 denotes a perfect negative relationship and +1.0 signifies a perfect positive relationship. A value of 0 indicates the absence of any linear relationship between the variables. The closer the coefficient is to either extreme, the stronger the correlation between the variables (David *et al*., 2018). Model accuracy is evaluated using the Kappa coefficient, where values between 0.81–1.00 indicate very good agreement, 0.61–0.80 good, 0.41–0.60 moderate, 0.21–0.40 fair, and <0.20 poor (Subiyanto & Suprayogi, 2019). Model parameters such as learning rate, hidden layers, momentum, and neighborhood were repeatedly adjusted to minimize validation errors (minimum validation overall error) (Hapsary *et al*., 2021).

Thus, the ANN in the MOLUSCE plugin operates by iteratively learning spatial transition patterns between land cover classes based on the driving variables (roads, rivers, built-up areas), enabling it to generate reliable projections of future land cover changes. Due to data limitations, external validation (comparison between the simulated and actual land cover) could not be performed. Model validation was instead based on internal assessment using the validation overall error and Kappa coefficient generated during the training process in the MOLUSCE plugin. A higher Kappa value indicates better model performance and higher reliability of the prediction results.

2.2.2. Curve Number, Impervious and Initial Abstraction Analysis

To estimate surface runoff, the Soil Conservation Service Curve Number (SCS-CN) method is a widely applied hydrological approach for watershed analysis. The determination of Curve Number (CN) values takes into account land cover, soil properties, and hydrologic soil group (HSG) classifications, which collectively represent the runoff potential of a given area (Hussain *et al*., 2024).

The first, soil data must first be classified into hydrologic soil groups (HSG) then overlays with land cover data, are then used to determine CN values. An overlay process between the land cover map and soil type map was carried out using ArcGIS software. The results of this overlay were used to determine the CN composites values and impervious composites percentages from each sub-watershed

CN values range from 0 to 100, where a CN of 100 indicates that rainfall is entirely converted into runoff without any infiltration, while a CN of 0 indicates that all rainfall infiltrates into the soil. A composite CN must be calculated when a watershed consists of multiple land cover types and soil groups (Wardhana *et al*., 2018). Changes in CN values also affect the percentage of land capacity to absorb rainfall at the surface, expressed as impervious (Marko & Zulkarnain, 2018).

Impervious surfaces represent a key form of artificial land cover. They alter rainfall runoff, infiltration, and evapotranspiration processes, thereby directly influencing the environment, ecosystems, biodiversity, and the likelihood of disasters at the regional scale (Zheng *et al*., 2023). The extent of impervious areas is influenced by watershed characteristics such as soil permeability and slope (Blum *et al*., 2020). An increase in impervious surfaces significantly impacts peak discharge and runoff volume (Gholami *et al*., 2010).

The Curve Number (*CN*) value influences the magnitude of rainfall losses at the beginning of a rainfall event (Initial Abstraction, *Ia*). A higher *CN* value corresponds to a smaller Ia value (Marko & Zulkarnain, 2018). The magnitude of Initial Abstraction (*Ia*) was calculated from maximum potential storage (Smax) using Equation (1):

$$Ia = 0.2\ Smax \tag{1}$$

The maximum potential storage (*Smax*) was calculated based on the *CN* value, using Equation (2):

$$S_{max} = \frac{25400-254CN}{CN} \tag{2}$$

2.2.3. Flood Discharge Analysis

Flood discharge analysis was conducted in the following stages:

- Rainfall stations were analyzed using the Thiessen Polygon method to determine the influence of each station and to calculate the average areal rainfall.
- The series of maximum daily flood discharge data and maximum daily rainfall data were tested for data quality using outlier and trend analysis methods (Badan Standardisasi Nasional, 2016).
- Rainfall design for each station and flood discharge design at the Cibendung stream gauge station were analyzed for return periods of 2, 5, 10, 20, 25, 50, and 100 years using the Normal, Log-Normal, Gumbel, and Log Pearson Type III methods, followed by frequency distribution tests using Chi-Square and Kolmogorov-Smirnov methods.
- The areal rainfall was subsequently adjusted using the Area Reduction Factor (ARF) to represent the temporal and spatial variability of rainfall events.
- Hourly rainfall distribution was analyzed using PSA-007 with a 6-hour duration. The Cijangkelok Watershed is classified as a medium-sized watershed (10–100 km²). For small and medium-sized watersheds with a concentration time of 2–3 hours, a 6-hour rainfall duration is recommended (Balai Teknik Bendungan, 2022).
- Rainfall–runoff analysis was conducted using the HEC-HMS software, applying the SCS and Snyder Unit Hydrograph methods with several input parameters, including CN, impervious, initial abstraction, time lag, and peak coefficient (Manual, 2023).

In the SCS Unit Hydrograph (SCS-UH) transformation analysis, the value of tlag is influenced by watershed slope, the length of the main river, concentration time, and maximum storage potential (USDA-NRCS, 2010) as expressed in Equations (3) and (4).

$$Tc = \frac{l^{0.8}(S_{max}+1)^{0.7}}{1.140\ Y^{0.5}} \tag{3}$$

$$t_{Lag} = 0.6\ T_c \tag{4}$$

where T_c is time of concentration (h), t_{Lag} is time lag from the onset of rainfall to the arrival of peak discharge in the river (h), L is length of the main river (feet), and Y is average watershed slope (%).

Whereas in the Snyder Unit Hydrograph transformation analysis, the value of t_{lag} is influenced by the length of the main river and centroid, the watershed characteristic coefficient, and the unit constant, as showed in Equation (5):

$$t_{Lag} = C_1 C_t\ (L\ L_c)^{0.3} \tag{5}$$

where L is length of the main river (km), Lc is length of the stream channel from the outlet to the point nearest to the centroid of the watershed (km), C_1 is unit constant (0.75 for SI units and 1.0 for English units), C_t is coefficient dependent on the shape and slope of the watershed, generally ranging from 1.0 to 2.2, where steeper watershed slopes correspond to smaller Ct values (Salami *et al*., 2017).

The results of the simulated flood discharge analysis in HEC-HMS were validated using observed flood discharge data from Water Level Station Cibendung. Parameter calibration in HEC-HMS was carried out to obtain optimal model parameters by comparing the simulated discharges from HEC-HMS with the observed discharges (Nadia *et al*., 2019). The correlation between the two discharge datasets was evaluated using the Percent Bias (PBIAS) and Nash-Sutcliffe Efficiency (NSE) methods, as expressed in Equations (6) and (7).

$$\text{PBIAS} = \left|\frac{\sum_i^n (Q_{obs} - Q_{sim})}{\sum_i^n Q_{obs}}\right| \times 100\% \quad (6)$$

$$\text{NSE} = 1 - \left[\frac{\sqrt{\sum_i^n (Q_{obs} - Q_{sim})^2}}{\sqrt{\sum_i^n (Q_{obs} - \overline{Q_{obs}})^2}}\right] \quad (7)$$

where n is number of data, Q_{obs} is observed flood discharge, Q_{sim} is simulated flood discharge.

A PBIAS value of zero indicates that the average simulated discharge is equivalent to the observed discharge. Meanwhile, the NSE value ranges from negative infinity to 1, where values closer to 1 indicate better agreement between the simulated and observed discharges (Malindo, 2022). The classification of PBIAS and NSE values is presented in Table 1.

Table 1. Evaluation of the performance of simulated and observed results

Performance Rating	PBIAS	NSE
Very Good	PBIAS < ±10	0.6<NSE≤1.0
Good	±10≤PBIAS < ±15	0.4<NSE≤0.6
Satisfactory	±15≤PBIAS < ±25	0.2<NSE≤0.4
Unsatisfactory	PBIAS ≥ ±25	NSE≤0.2

Source: (Moriasi *et al*., 2007; Cabrera, 2009)

3. RESULTS AND DISCUSSION

3.1. Land Cover Prediction Analysis

The input data in the modeling process consisted of the 2009 land cover map as the initial condition and the 2022 land cover map as the final condition. The driving variables employed were distance to roads, distance to rivers, and distance to built-up areas, under the assumption that development is likely to occur in areas surrounding roads, rivers, and built-up areas. The driving variables were statistically tested using Pearson's correlation method, with the results presented in Table 2.

Table 2. Correlation test results

	River	Road	Built-up area
River	1	0.391	0.718
Road	0.391	1	0.804
Built-up area	0.718	0.804	1

Based on Table 2, the correlation between rivers and built-up areas as well as roads and built-up areas shows values approaching 1. This suggests a spatial association between proximity to built-up areas and land cover transition. Subsequently, the results from the MOLUSCE analysis were used to examine the changes in initial and final land cover, as presented in Table 3. The land cover class that experienced the largest decrease was dryland agriculture mixed with shrubs, which declined by 35.5 km², while the largest increase occurred in rice fields, with an addition of 18.8 km². Over the course of 13 years, most dryland agriculture mixed with shrubs was converted into rice fields.

MOLUSCE further generated a transition matrix depicting the likelihood of land cover change. The analysis showed that the most stable classes were secondary dryland forest (98.74%) and plantations (96.85%). In contrast, dryland agriculture retained only 47.09%, with major conversions to rice fields (32.61%) and dryland agriculture mixed

Table 3. Land Cover Changes (2009–2022)

Land Cover Changes	Area (km²)		Changes (km²)
	2009	2022	
Secondary dryland forest	18.9	23.0	4.1
Plantation forest	54.8	63.1	8.3
Dryland agriculture	16.7	17.0	0.9
Mixed dryland agriculture with shrubs	39.5	4.0	-35.5
Rice fields	12.2	31.0	18.8
Plantation	0.3	2.7	1.9
Built-up area	4.6	6.7	2.1

with shrubs (7.13%). The latter was even less stable, with only 20.09% persisting and the largest transitions occurring to rice fields (40.59%) and dryland agriculture (20.09%), indicating that these two classes are the most dynamic in terms of change.

Furthermore, the transition potential modeling employed the Artificial Neural Network (ANN) method with input parameters consisting of a learning rate of 0.001, momentum of 0.001, a maximum of 500 iterations, and 10 hidden layers. This configuration produced a land cover prediction with a minimum validation overall error of 0.0332 and a validation Kappa of 0.765. These values indicate a good level of accuracy; thus, the 2035 land cover prediction can be utilized for further analysis, although it still presents certain limitations in terms of validation. The land cover conditions for 2009, 2022, and the 2035 prediction processed in QGIS are illustrated Figure 2.

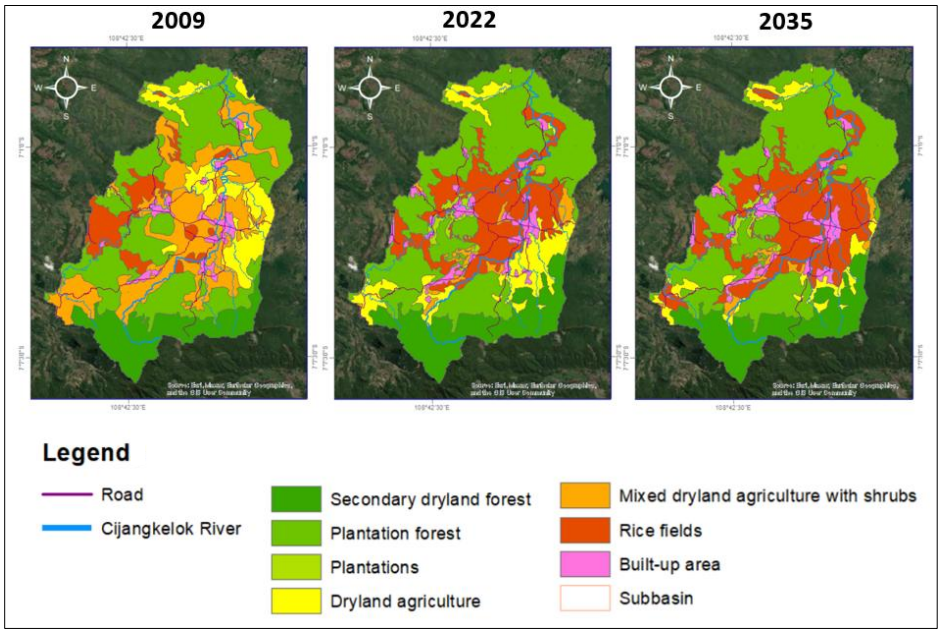

Figure 2. Land cover 2009, 2022, and 2035 prediction

It is evident that there is a dynamic shift in land cover, particularly marked by the expansion of rice fields. The quantitative details of these land cover changes are presented in Table 4. The results indicate that in the projected 2035 land cover, a significant shift in land utilization occurs. Reductions are observed in dryland agriculture (7.1 km²), mixed dryland agriculture with shrubs (3.6 km²), and plantations (0.1 km²), which are simultaneously replaced by an expansion of rice fields (8.4 km²), built-up areas (1.3 km²), plantation forest (1.1 km²), and secondary dryland forest (0.1 km²). This confirms a transition in land cover dominance from dryland agriculture and mixed dryland agriculture with shrubs and toward rice fields, built-up areas, and forest plantations.

Table 4. Land cover changes in the Cijangkelok Watershed (2009 - 2022 - 2035)

No	Land Cover Type	Area (km²)			Changes 2022 to 2035 (km²)
		2009	2022	2035	
1	Secondary dryland forest	18.9	23.0	23.0	+0.1
2	Plantation forest	54.8	63.1	64.2	+1.1
3	Dryland agriculture	16.7	17.0	9.9	-7.1
4	Mixed dryland agriculture with shrubs	39.5	4.0	0.4	-3.6
5	Rice fields	12.2	31.0	39.4	+8.4
6	Plantation	0.3	2.3	2.1	-0.1
7	Built-up area	4.6	6.7	8.0	+1.3
	TOTAL	**147.1**	**147.1**	**147.1**	

3.2. Curve Number, Impervious dan Initial Abstraction Analysis

The Curve Number (CN) values were determined based on the analysis of hydrologic soil groups (HSG) and land cover, following the standards established by the USDA (1986). According to the HWSD from FAO, the Cijangkelok watershed is dominated by two soil types: mediterranean soils 66.1% and grumusol soils 33.9%. Mediterranean soils belong to Hydrologic Soil Group B, characterized by a dominant sand mixture with small amounts of clay and silt, and a moderate rate of water transmission. In contrast, Grumusol soils fall under Hydrologic Soil Group D, dominated by clay particles, which have very low water transmission and a high potential for runoff generation.

Subsequently, an overlay process between the land cover map and soil type map was carried out using ArcGIS software. The results of this overlay were used to determine the CN composites values and impervious composites percentages from each sub-watershed, as presented in Tables 5. Based on the derived CN composite values, the Initial Abstraction (Ia) was calculated in accordance with the SCS method, with the results shown in Table 5.

Table 5. Curve Number (CN) composite, Impervious composite, and Initial Abstraction values

Parameter	Year		
	2009	2022	2035
CN composite	67.9	68.0	68.4
Impervious composite	5.6	5.7	6.3
Initial Abstraction	24.0	23.9	23.5

The composite CN values exhibit an increasing trend, although not significantly, indicating a reduced capacity of the watershed to infiltrate water due to land cover changes. Similarly, the composite impervious values also show an upward trend, reflecting the expansion of impermeable areas in line with built-up land development. Meanwhile, the initial abstraction values tend to decline, suggesting a decreasing initial capacity of the watershed to retain runoff. Overall, the combination of increasing CN and impervious values along with decreasing initial abstraction highlights the potential for greater surface runoff in the future. These values were subsequently used as inputs in the loss analysis within HEC-HMS.

3.3. Flood Discharge Analysis

Based on the Thiessen polygon analysis, six rainfall stations were found to influence the Cijangkelok Watershed, as shown in Figure 3. The Thiessen coefficients for each station are as follows: Ciwaru 0.26, Luragung 0.08, Cikeusik 0.02, Cibendung 0.41, Malahayu 0.41, and Kertasari 0.09. The annual maximum daily rainfall values for each rainfall station are presented in Table 6.

The data quality of the six rainfall stations was evaluated using outlier and trend tests, and the results indicated that no outliers or anomalies were present in any of the rainfall records. Design rainfall was then calculated for each station with return periods of 2, 5, 10, 20, 25, 50, and 100 years using the Normal, Gumbel, Log-Normal, and Log Pearson Type III methods. Based on the Chi-Square and Smirnov–Kolmogorov goodness-of-fit tests, and considering the smallest error value of 3.67%, the Gumbel method was selected as the most appropriate distribution.

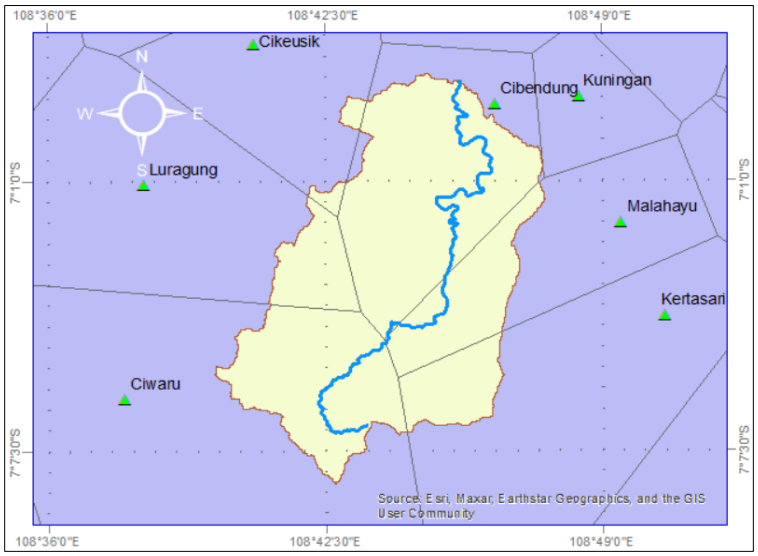

Figure 3. Thiessen Polygon distribution of rainfall stations in the Cijangkelok Watershed

Table 6. Annual maximum daily rainfall

Year	Ciwaru	Luragung	Cikeusik	Cibendung	Malahayu	Kertasari
2005	95	90	108	110	131	70
2006	95	140	71	105	108	87
2007	81	74	98	123	123	108
2008	93	60	85	118	137	108
2009	108	65	99	74	96	140
2010	60	70	122	120	105	170
2011	79	70	87	147	145	140
2012	82	71	152	92	90	115
2013	93	65	120	142	120	96
2014	78	102	92	116	124	94
2015	90	73	97	111	126	97
2016	98	73	90	111	99	97
2017	136	150	110	125	102	114
2018	95	68	117	107	160	89
2019	105	58	126	92	78	110
2020	74	103	103	124	102	105
2021	77	84	131	105	135	137
2022	92	97	85	78	81	110
2023	77	95	87	85	131	63
2024	105	99	88	94	97	75

Table 7. Design rainfall based on Gumbel method in each rainfall station for different return period

Return Period (year)	Design Rainfall (mm)					
	Ciwaru	Luragung	Cikeusik	Cibendung	Malahayu	Kertasari
2	88.5	81.8	100.2	105.8	110.9	102.0
5	103.0	104.3	117.6	122.8	130.4	124.9
10	112.6	119.2	129.2	134.1	143.2	140.0
20	121.8	133.5	140.3	145.0	155.6	154.5
25	124.7	138.1	143.8	148.4	159.5	159.2
50	133.7	152.0	154.6	159.0	171.6	173.4
100	142.7	165.9	165.4	169.5	183.6	187.4

The rainfall area was obtained by multiplying the design rainfall at each station with the Thiessen coefficient. The results then adjusted using the Area Reduction Factor (ARF), a correction factor applied to convert point rainfall into a more representative value for a larger catchment area. With a watershed area of 147.1 km², the ARF value was determined to be 0.885. The result of areal design rainfall as presented in Table 8.

Table 8. Areal design rainfall

Return Period (year)	Areal Design Rainfall (mm)	Areal design rainfall × ARF (mm)
2	99.6	88.1
5	117.3	103.8
10	129.0	114.1
20	140.2	124.1
25	143.8	127.2
50	154.8	136.9
100	165.7	146.6

Table 9. Hourly rainfall distribution for return period 2 year (Q02) to 100 year (Q100)

Time	Hourly Rainfall Distribution (mm)						
	Q02	Q05	Q10	Q20	Q25	Q50	Q100
1	4.4	5.2	5.7	6.2	6.4	6.9	7.3
2	8.8	10.9	11.4	12.4	12.7	13.7	14.7
3	52.9	62.7	68.5	74.4	76.3	82.2	87.9
4	14.1	16.6	18.3	19.8	20.4	21.9	23.5
5	5.3	6.2	6.8	7.4	7.6	8.2	8.8
6	2.6	3.1	3.4	3.7	3.8	4.1	4.4

The study watershed, with an area of 147.12 km², falls into the category of a medium-sized watershed; therefore, a 6-hour rainfall distribution was applied. The hourly rainfall distribution method used is PSA-007, in accordance with the guidelines of Balai Teknik Bendungan (2002), with the rainfall distribution presented in Table 9. Using HEC-HMS modeling, flood discharges for the years 2009, 2022, and 2035 were simulated with the SCS and Snyder Unit Hydrograph methods for several return periods, and the results are presented in Table 10.

Table 10. Simulated flood discharge based on SCS UH and Snyder UH methods

Return Period (year)	Simulated flood discharge (m³/s)					
	SCS UH method			Snyder UH method		
	2009	2022	2035	2009	2022	2035
2	351.2	354.6	366.1	353.6	353.7	360.2
5	453.3	457.9	471.8	456.3	456.6	464.1
10	524.2	529.7	545.2	527.9	528.0	536.2
20	594.5	600.9	617.8	598.5	598.8	607.5
25	617.2	623.8	641.3	621.3	621.6	630.5
50	688.2	695.7	714.6	692.6	693.0	702.5
100	760.3	768.7	789.0	764.9	765.4	775.4

The percentage increase in flood discharge from 2009 to 2035 is relatively small for both the SCS UH and Snyder UH methods, generally less than 2%. In the SCS UH method, the average increase in flood discharge during both the 2009–2022 and 2022–2035 periods is relatively similar, at around ±6 m³/s. Meanwhile, in the Snyder UH method, the increase in discharge for the 2009–2022 period is very small, only about ±0.3 m³/s, whereas in the 2022–2035 period the increase is larger, reaching about ±8.5 m³/s.

To assess the agreement between simulated design discharge and frequency-based discharge estimates, an analysis was conducted using observed discharge data. This analysis aims to evaluate the river flow characteristics based on historical data, so that it can be used as a reference for comparison with the hydrological model results.

The maximum annual daily discharge data over 14 years (2011–2024) was tested for quality using outlier and trend tests, with the results showing no outliers or trends. Subsequently, design discharges for return periods of 2, 5, 10, 20, 25, 50, and 100 years were analyzed using the Normal, Gumbel, Log-Normal, and Log-Pearson Type III methods. Based on the Chi-Square and Smirnov-Kolmogorov tests, as well as considering the smallest error value, the Gumbel method was selected as the best method. The design discharges for various return periods using the Gumbel method are shown in Table 11.

Table 11. Design discharge based on Gumbel method for different return periods for Water Level Station Cibendung

Return Period (year)	Discharge (m^3/s)
2	403.6
5	491.4
10	549.5
20	605.2
25	622.9
50	677.4
100	731.5

To optimize the model parameters, the simulated flood discharge for 2022 was compared with the design discharge at return period 25 year (Q25). Although the regulation suggests Q20 for district-scale design, Q25 was used to obtain a more conservative and reliable estimation considering data uncertainty, climate change impacts, and safety requirements in flood-prone areas. The validation results were evaluated using the NSE and PBIAS methods, as shown in Table 12 and Table 13.

Table 12. Statistical comparison of discharge between frequency-based and simulated SCS UH design

Return Period	Flood Discharge (m^3/s)		PBIAS (%)		NSE	
(year)	Design Gumbel	SCS UH Simulated	Value	Interpretation	Value	Interpretation
2	403.6	354.6	12.1	Good	1.0	Very good
5	491.4	457.9	6.8	Very good	1.0	Very good
10	549.5	529.7	3.6	Very good	1.0	Very good
20	605.2	600.9	0.7	Very good	1.0	Very good
25	**622.9**	**623.8**	**0.1**	**Very good**	**1.0**	**Very good**
50	677.4	695.7	2.7	Very good	1.0	Very good
100	731.5	768.7	5.1	Very good	1.0	Very good

Table 13. Statistical comparison of discharge between frequency-based and simulated Snyder UH design

Return Period	Flood Discharge (m^3/s)		PBIAS (%)		NSE	
(year)	Design Gumbel	SCS UH Simulated	Value	Interpretation	Value	Interpretation
2	403.6	353.7	12.4	Good	1.0	Very good
5	491.4	456.6	7.1	Very good	1.0	Very good
10	549.5	528.0	3.9	Very good	1.0	Very good
20	605.2	598.8	1.1	Very good	1.0	Very good
25	**622.9**	**621.6**	**0.2**	**Very good**	**1.0**	**Very good**
50	677.4	693.0	2.3	Very good	1.0	Very good
100	731.5	765.4	4.6	Very good	1.0	Very good

The comparison results show a high statistical agreement between design discharge magnitude and simulated values using both the SCS UH and Snyder UH methods. Most PBIAS values are < 10% (except for return period 2 year), indicating relatively small errors, and NSE values are 1.0, which fall into the very good category. Compared to the Snyder UH method, the SCS UH method produces results that are closer to the design discharge, as indicated by the lower PBIAS values in almost all return periods.

Changes in hydrological characteristics due to land cover shifts are reflected in the magnitude of the design flood discharge. Based on the SCS UH method with a 25-year return period, the flood discharges in 2009, 2022, and 2035 are 617.2 m^3/s, 623.8 m^3/s, and 641.3 m^3/s, respectively, with a percentage increase of 2.9% (between 2022-2035). Meanwhile, in the same years, the Snyder UH method produced flood discharges of 621.3 m^3/s, 621.6 m^3/s, and 630.5 m^3/s, with a percentage increase of 1.5% (between 2022-2035). These results indicate that land cover changes contribute to the increased potential for future flooding. However, the changes in discharge are not substantial, as most of the land cover changes were converted into rice fields, which have the capacity to retain water flow, thereby reducing immediate surface runoff.

4. CONCLUSIONS

Overall, the analysis results indicate that in the Cijangkelok watershed there has been an increase in flood discharge within a 13-year period of approximately ±1.5–2.9%. This suggests that land cover changes contribute to the increase in flood discharge, although the impact is not highly significant because most of the land cover changes were converted into rice fields, which have the capacity to retain water flow, thereby reducing immediate surface runoff.

The land cover condition in 2035 used in this analysis is only a prediction. Future changes may differ from the projection results, depending on the dynamics of economic development, political policies, and community activities that may affect land use patterns. This analysis is still preliminary as it only considers land cover change factors. Further studies are needed to also incorporate other aspects such as changes in rainfall due to climate change, watershed morphometric characteristics, and river hydraulics conditions. With a more comprehensive approach, future flood discharge projections can be illustrated more accurately and closer to real conditions.

AUTHOR CONTRIBUTION STATEMENT

Author	C	M	So	Va	Fo	I	R	D	O	E	Vi	Su	P	Fu
VF	✓	✓	✓	✓	✓	✓	✓	✓	✓	✓		✓	✓	✓
YS	✓	✓		✓	✓		✓					✓		
TWA			✓			✓		✓						
AYW						✓		✓			✓			
YPS					✓				✓	✓	✓		✓	

C: Conceptualization	Fo: Formal Analysis	O: Writing - Original Draft	Fu: Funding Acquisition
M: Methodology	I: Investigation	E: Writing - Review & Editing	P: Project Administration
So: Software	D: Data Curation	Vi: Visualization	
Va: Validation	R: Resources	Su: Supervision	

REFERENCES

Anggista, D., Zahra, F.A., Mariani, N., & Winasis, A. (2025). Capacity Analysis of downstream Cijangkelok River using HEC-RAS software. *Indonesian Journal of Advanced Research, **4***(7), 1543–1558. https://doi.org/10.55927/ijar.v4i7.14965

BSN (Badan Standardisasi Nasional). (2016). *Tata Cara Perhitungan Debit Banjir Rencana* (SNI 2415:2016). Badan Standardisasi Nasional.

Balai Teknik Bendungan. (2022). *Modul 1 - Analisis Curah Hujan*. Direktorat Jenderal Sumber Daya Air, Kementerian PUPR.

Blum, A.G., Ferraro, P.J., Archfield, S.A., & Ryberg, K.R. (2020). Causal effect of impervious cover on annual flood magnitude for the United States. *Geophysical Research Letters, **47***(5), e2019GL086480. https://doi.org/10.1029/2019GL086480

Cabrera, J. (2009). *Calibración de Modelos Hidrológicos*. IMEFEN – Universidad Nacional de Ingeniería. https://www.imefen.uni.edu.pe/Temas_interes/modhidro_2.pdf

Carsono, N. (2021). Analisis debit banjir Sungai Cijangkelok di Desa Cibingbin Kecamatan Cibingbin Kabupaten Kuningan. *Syntax Literate: Jurnal Ilmiah Indonesia, **6***(4). https://doi.org/10.36418/syntax-literate.v6i4.2469

David, S.J., Shaji, A., Ashmy, M.S., Raju, N., & Sebastian, N. (2018). A novel methodology for infiltration model studies. *International Journal of Engineering Technologies and Management Research,* ***5***(3), 190–199. https://doi.org/10.29121/ijetmr.v5.i3.2018.191

Gholami, V., Mohseni Saravi, M., & Ahmadi, H. (2010). Effects of impervious surfaces and urban development on runoff generation and flood hazard in the Hajighoshan watershed. *Caspian Journal of Environmental Sciences,* ***8***(1), 1–12.

Hapsary, M.S.A., Subiyanto, S., & Firdaus, H.S. (2021). Analisis prediksi perubahan penggunaan lahan dengan pendekatan artificial neural network dan regresi logistik di Kota Balikpapan. *Jurnal Geodesi Undip,* ***10***(2), 88–97. https://doi.org/10.14710/jgundip.2021.30637

He, J., Wan, Y.-R., Chen, H.-T., & Wang, W.-C. (2021). Study on the impact of land-use change on runoff variation trend in Luojiang River Basin, China. *Water,* ***13***(22), 3282. https://doi.org/10.3390/w13223282

Hussain, J.K.N., Channavar, V.R., Malappanavar, N., Radder, V.S., Chandrakar, T., Jagadeesh, B.R., & Basavaraj, D.B. (2024). Spatial analysis of surface runoff using SCS-CN technique integrated with GIS and remote sensing. *International Journal of Environment and Climate Change,* ***14***(5), 441–454. https://doi.org/10.9734/ijecc/2024/v14i54204

Kamaraj, M., & Rangarajan, S. (2022). Predicting the future land use and land cover changes for Bhavani basin, Tamil Nadu, India, using QGIS MOLUSCE plugin. *Environmental Science and Pollution Research,* ***29***, 86337–86348. https://doi.org/10.1007/s11356-021-17904-6

Malindo, D. (2022). *Bimbingan Teknis Analisis Debit Banjir Desain dengan Menggunakan Data Hujan Satelit (TRMM/GPM)*. Balai Teknik Bendungan – Ditjen SDA.

Manual, H.T.R. (2023). *HEC-HMS Technical Reference Manual*. Hydrologic Engineering Center.

Marko, K., & Zulkarnain, F. (2018). Pemodelan debit banjir sehubungan dengan prediksi perubahan tutupan lahan di Daerah Aliran Ci Leungsi Hulu menggunakan HEC-HMS. *Jurnal Geografi Lingkungan Tropik,* ***2***(1), 3. https://doi.org/10.7454/jglitrop.v2i1.31

Moriasi, D.N., Arnold, J.G., Van Liew, M.W., Bingner, R.L., Harmel, R.D., & Veith, T.L. (2007). Model evaluation guidelines for systematic quantification of accuracy in watershed simulations. *Transactions of the ASABE,* ***50***(3), 885–900. https://doi.org/10.13031/2013.23153

Muhammad, R., Zhang, W., Abbas, Z., Guo, F., & Gwiazdzinski, L. (2022). Spatiotemporal change analysis and prediction of future land use and land cover changes using QGIS MOLUSCE plugin and remote sensing big data: A case study of Linyi, China. *Land,* ***11***(3). https://doi.org/10.3390/land11030419

Nadia, K., Mananoma, T., & Tangkudung, H. (2019). Analisis debit banjir dan tinggi muka air Sungai Tembran di Kabupaten Minahasa Utara. *Jurnal Sipil Statik*, *7*(6), 703–710.

Rahayu, R., Mathias, S.A., Reaney, S., Vesuviano, G., Suwarman, R., & Ramdhan, A.M. (2023). Impact of land cover, rainfall and topography on flood risk in West Java. *Natural Hazards, 116*, 1735–1758. https://doi.org/10.1007/s11069-022-05737-6

Salami, W.A., Bilewu, S.O., Ibitoye, B.A., & Ayanshola, M.A. (2017). Runoff hydrographs using Snyder and SCS synthetic unit hydrograph methods: A case study of selected rivers in South West Nigeria. *Journal of Ecological Engineering,* ***18***(1), 25–34. https://doi.org/10.12911/22998993/66258

Sjarief, A.W.P., & Lasminto, U. (2020). Analysis of water surface profile and flood discharge of Cijangkelok river. *IOP Conference Series: Materials Science and Engineering,* ***930***, 012079. https://doi.org/10.1088/1757-899X/930/1/012079

Subiyanto, S., & Suprayogi, A. (2019). Modeling and spatial analysis of change settlement and fair market land price using Markov chain model in Banyumanik District. *KnE Engineering,* ***4***(3), 278–290. https://doi.org/10.18502/keg.v4i3.5866

USDA–NRCS. (2010). *National Engineering Handbook: Part 630 Hydrology, Chapter 15 – Time of concentration*. United States Department of Agriculture, Natural Resources Conservation Service.

Wardhana, P. N., Astuti, S. A. Y., & Kurnia, D. (2018). Pengaruh perubahan tutupan lahan terhadap debit banjir di DAS Winongo Daerah Istimewa Yogyakarta. *Jurnal Ilmiah Teknik Sipil*, ***22***(2).

Yoani, A., Sediono, S., Mardianto, M.F.F., & Pusporani, E. (2023). Prediction of monthly flood occurrences in Indonesia based on long short term memory analysis. *G-Tech: Jurnal Teknologi Terapan,* ***7***(4). https://doi.org/10.33379/gtech.v7i4.3346

Zheng, K., He, G., Yin, R., Wang, G., & Long, T. (2023). A comparison of seven medium resolution impervious surface products on the Qinghai–Tibet Plateau, China from a user's perspective. *Remote Sensing*, ***15***(9), 2366. https://doi.org/10.3390/rs15092366